# Preparation and characterization of AuNPs/CNTs-ErGO electrochemical sensors for highly sensitive detection of hydrazine

Zhenting Zhao, Yongjiao Sun, Pengwei Li, Wendong Zhang, Kun Lian, Jie Hu, Yong Chen

# Preparation and characterization of AuNPs/CNTs-ErGO electrochemical sensors for highly sensitive detection of hydrazine

Zhenting Zhao[a], Yongjiao Sun[a], Pengwei Li[a], Wendong Zhang[a], Kun Lian[a], Jie Hu[a*], Yong Chen[b]*

[a]Mcro and Nano System Research Center, Key Lab of Advanced Transducers and Intelligent Cont rol System (Ministry of Education) & College of Information Engineering, Taiyuan University of Technology, Taiyuan 030024, Shanxi, China

[b]Ecole Normale Supérieure, CNRS-ENS-UPMC UMR 8640, Paris 75005, France

Email: hujie@tyut.edu.cn (J. Hu)

yong.chen@ens.fr (Y. Chen)

*Author for correspondence.



## Abstract

A highly sensitive electrochemical sensor of hydrazine has been fabricated by Au nanoparticles (AuNPs) coating of carbon nanotubes-electrochemical reduced graphene oxide composite film (CNTs-ErGO) on glassy carbon electrode (GCE). Cyclic voltammetry and potential amperometry have been used to investigate the electrochemical properties of the fabricated sensors for hydrazine detection. The performances of the sensors were optimized by varying the CNTs to ErGO ratio and the quantity of Au nanoparticles. The results show that under optimal conditions, a sensitivity of 9.73 $\mu A \cdot \mu M^{-1} \cdot cm^{-2}$, a short response time of 3 s, and a low detection limit of 0.065 μM could be achieved with a linear concentration response range from 0.3 μM to 319 μM. The enhanced electrochemical performances could be attributed to the synergistic effect between AuNPs and CNTs-ErGO film and the outstanding catalytic effect of the Au nanoparticles. Finally, the sensor was successfully used to analyse the tap water, showing high potential for practical applications.

## Graphical abstract

A highly sensitive hydrazine electrochemical sensor was fabricated by using carbon nanotubes and electrochemical reduced graphene oxide composite film (CNTs-ErGO) and surface deposition of Au nanoparticles (AuNPs).

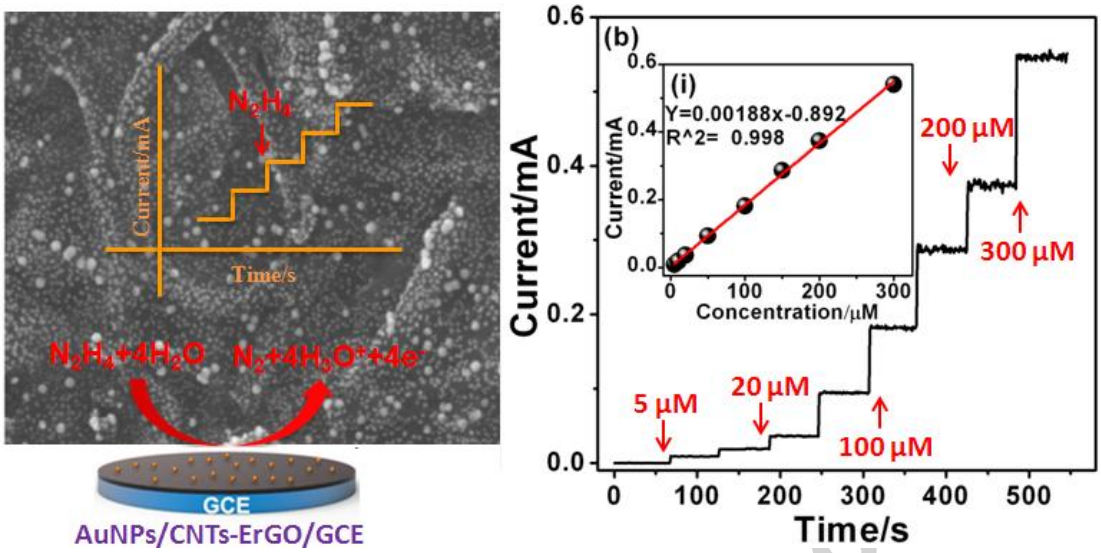


**Keywords:** Reduced graphene oxide, Carbon nanotubes, Au nanoparticles, Hydrazine sensor

## 1. Introduction

Hydrazine and its derivatives are widely used as antioxidants, corrosion inhibitors, rocket propellants, fuel cells, pesticides, plant growth regulators and so on [1-5]. However, hydrazine is highly toxic and dangerously unstable unless handled in solution. Exposure of hydrazine may lead to irritation of nose, eyes, throat, headache, nausea etc. Acute exposure can cause kidney, liver and central nervous system damage [6-8]. According to the U.S. Department of Labor Occupational Safety & Health Administration and Environmental Protection Agency, the concentration of hydrazine in workplace air should be below 0.03 μg/mL for a 2-h period [9, 10]. Therefore, it is important to develop high sensitive method for the determination and quantification of hydrazine. Among different approaches [11-15], the electrochemical oxidation technique showed unique advantages of simple, accurate and cost effective

[5, 16]. However, the electrochemical detection of hydrazine using for conventional electrodes requires a relatively high over-potential. Efforts were then devoted to the minimization of the over-potentials and the increase of the oxidation current response by using such as carbon nanomaterials, metal or metal oxide nanostructures as electron mediators immobilized on conventional electrodes [11, 17, 18].

Recently, considerable attention has been paid to the use of two-dimensional carbon nanomaterial with single atomic layer of graphene for hydrazine detection, owing to their excellent properties such as good electrical conductivity, large surface area, strong mechanical strength and a wide electrochemical window [19-21]. For example, Takahashiet al. used reduced graphene oxide (rGO)-modified glass carbon electrode (GCE) to evaluate the electrochemical response of hydrazine and achieved a linear concentration range of 10-100 μM [22]. Wang et al. fabricated a hydrazine electrochemical sensor with high surface area graphene, which showed a linear response range of 3.0-300 μM and a detection limit of 1.0 μM [23]. Mutyala et al. reported a hydrazine detection sensitivity of 0.028 μA/μM and a linear range of 0.5-7.5 μM by using graphene nanoflakes [24]. On the other hand, metal nanoparticles and carbon nanotubes have been introduced to further improvement the electrocatalytic activity of graphene for hydrazine detection [25-27]. Wang et al. used graphene supported Bi nanoparticles and demonstrated a linear range of 0.02-280 μM [28]. Qin et al. also demonstrated the suitability of using AuNPs/rGO nanocomposites for hydrazine detection, showing a linear concentration range of 5-900 μM and a detection limit of 0.12 μM [29]. Similarly, Mani et al. developed GO-CNT-FePc modified electrodes and showed a linear concentration range of 0.5-83.5 μM with a detection limit of 0.093 μM [30]. Nevertheless, the overall performances of those sensors are not ideal for the trace hydrazine detection.

In this work, we report the development of Au nanoparticles coated carbon nanotubes-reduced graphene oxide composite film on glassy carbon electrode for the trace level detection of hydrazine. The weight ratio of CNTs to GO and the deposition time of Au nanoparticles were optimized by evaluating the electrocatalytic performance the sensors for hydrazine detection using cyclic voltammetry and amperometry techniques. As expected, the optimized electrochemical sensor exhibits a high sensitivity, wide linear range, short response time and a low detection limit for hydrazine trace analyses.

# 2. Experimental

## 2.1 Materials

The graphite (325 meshes) was purchased from Qingdao Huatai Lubricating and Sealing Science and Technology Co. Ltd. The multi-wall carbon nanotubes (purity > 95wt%, length: 10-30 μM, electrical conductivity: >100 S/cm) were obtained from Chengdu organic chemicals Co. Ltd. Chinese academy of sciences. Hydrochloric acid (HCl, 37.5%), sulfuric acid ($H_2SO_4$, 98%), potassium permanganate ($KMnO_4$), hydrogen peroxide ($H_2O_2$, 30%), ammonia ($NH_3 \cdot H_2O$, 28%), chloroauric acid ($HAuCl_4$), sodium dihydrogen phosphate ($NaH_2PO_4$) and disodium hydrogen phosphate ($Na_2HPO_4$) were all analytically pure grade and purchased from Sigma (USA). Deionized water (>18 MΩ) was obtained from a Milli-Q water-purification system (Millipore, France). The 0.1 M phosphate buffer solutions (PBS) were prepared by varying the ratio of $NaH_2PO_4$, $Na_2HPO_4$ and HCl.

## 2.2 Synthesis of graphene oxide

Graphene oxide (GO) was synthesized by a modified Hummers method [31]. In a typical process, the mixtures of graphite (1.0 g) and $KMnO_4$ (1.0 g) were added into 30 mL $H_2SO_4$ (98%) and stirred for 10 min at room temperature. Then the whole reactants were stirred for another 3.5 hours at 50 ℃. After that, the mixtures were further treated with 300 mL deionized water and 20 mL $H_2O_2$, then filtered and washed successively with 10% HCl aqueous solution completely until sulfate could not be detected by the qualitative test with $BaCl_2$. The resulting solid filtration residue was added into 300 mL deionized water and ultrasonic for 1 hour. Finally, the aqueous phase dispersion of graphene oxide can be obtained by centrifugation, and the concentration of the prepared GO solution was about 0.5 mg/mL.

## 2.3 Fabrication of modified electrode

Prior to the modification, the surface of the GCE (0.19625 $cm^2$) was firstly polished using alumina particles with a size of 1.0 μm, 0.3 μm, and 50 nm. After that, the GCE was sonicated in diluted nitric acid (1:1), acetone, anhydrous ethanol and deionized water (each for 10 min), sequentially. Different amounts of CNTs were dispersed in 5.0 mL GO solution by ultrasound agitation to form different concentrations of slurry.

Then the slurry was dropped onto the GCE and dried at room temperature for 1.5 hours. Subsequently, the GO was reduced at the potential range from -1.6 V to 0.0 V in PBS (pH=5.0) [32-34]. The electrochemical reduction process (CV curves) for pristine GO and CNTs-GO are shown in Fig. S1 (Supplementary Information). After that, the Au nanoparticles were electrodeposited on the surface of CNTs-ErGO/GCE at -0.25 V in 0.5 M $H_2SO_4$ containing 25 mM $HAuCl_4$. Fig. 1 illustrates the detail fabrication process of AuNPs/CNTs-ErGO/GCE electrode. Meanwhile, the electrochemical workstation (Zahner, IM6) was introduced to evaluate the sensing performances of the as-prepared AuNPs/CNTs-ErGO/GCE hydrazine electrochemical sensor, and the AuNPs/CNTs-ErGO/GCE, Pt wire and Ag/AgCl (3.5 M KCl) were used as the working electrode, the counter electrode and the reference electrode, respectively.

### 2.4 Instrumentation

The morphological features of the synthesized GO and AuNPs/CNTs-ErGO were investigated using atomic force microscopy (AFM, Park NX10) and scanning electron microscopy (SEM, JSM-7001F), separately. The crystallinity and crystal phases were measured by X-ray powder diffraction (XRD, Hao Yuan DX2700, Cu-K$\alpha_1$, $\lambda$=1.5406 Å). The chemical composition was analyzed using energy dispersive spectroscopy (EDS, QUANTAX200) with a 15 kV accelerating voltage.

## 3. Results and discussion

### 3.1 Characterization of GO, CNTs-GO and AuNPs/CNTs-ErGO

The as-synthesized GO was characterized by atomic force microscopy and X-ray powder diffraction. Fig. S2 presents the AFM image and height profiles of GO from dilute solution. The size of the GO sheets range from several tens of nanometers to micrometers, and the thickness is about 0.95 nm, which are consistent well with previously reported work [35]. In addition, the GO was also characterized by X-ray powder diffraction (XRD) as displayed in Fig. S2(b). The strongest peak of 2θ is the characteristic peak of the graphene oxide, indicating the layer spacing increased significantly compared with the graphite (2θ=25.6°). This is attributed to the introduction of oxygen-containing functional groups (hydroxyl, carboxyl, epoxy, etc.) between the graphite intercalation.

Fig. 2a exhibits the SEM images of GO, which reveals a wrinkled texture, and associates with the presence of flexible and thin GO nanosheets. Fig. 3b shows the morphology of carbon nanotubes with diameter of about 60-90 nm. Fig. 2(c-d) present the different magnification SEM images of CNTs-GO. Compared with the CNTs and GO, the CNTs-GO film provides a more efficient electrode surface for loading Au nanoparticles, which can also contribute to accelerate electron transfer between the analyte and modified electrode. Fig. 3 illustrates the general morphology of the deposited AuNPs on the CNTs-ErGO (2:1 in weight ratio) surface with different deposition times. It was quite evidence that the number and size of the AuNPs were apparently depending on the deposition time. Obviously, after deposition 5 s (Fig. 3a), there are just a small amount of AuNPs distributed on the surface of CNTs-ErGO, and the average diameter is about 12 nm (Fig. S3). Increasing the deposition time from 20 s to 80 s, the number and size of AuNPs are apparent increased as shown in Fig. 3(b-d). After deposition 120 s, the size of AuNPs could reach to 45 nm and the nanoparticles also began to aggregate together (Fig. 3e). When the deposition time reaches to 160 s, the diameter of AuNPs is about 77 nm (Fig. 3f). At the same time, the energy dispersive spectroscopy (EDS) was employed to investigate the chemical composition of AuNPs/CNTs-ErGO, and the measured results confirm the existence of C and Au without any detectable impurity element (Fig. S4).

**3.2 Effects of the weight ratio (CNTs:ErGO) on hydrazine catalytic**

To obtain the optimum weight ratio of CNTs:ErGO, different proportion of CNTs-ErGO mixture (CNTs: ErGO = 0:1, 0.5:1, 1:1, 1.5:1, 2:1, 3:1 and 4:1) were coated on the surface of GCE for hydrazine detection. From the photographs of CNTs-GO (Fig. S5), we can observe that the color of the mixture become darker with the increase of CNTs. The morphologies of these samples are shown in Fig. S6, which displays a relatively dense and uniform network nanostructure. Moreover, with the increasing ratio of CNTs, many CNTs appear on the surface of CNTs-ErGO film to form nanoscale pores. In order to evaluate the electrochemical properties, cyclic voltammetry was used to determine the sensitivities for different ratios of CNTs-ErGO. During the period of experiment, the as-prepared CNTs-ErGO electrodes were exposed to different concentrations of hydrazine in 0.1 M PBS (pH=7.4), and the sensitivity was estimated by the slope values, which derived from linear plots of oxidation peak currents vs. hydrazine concentrations (Fig. S7). The measured results

show that the sensitivity of the pure ErGO is only 0.102 μA/μM with an oxidation potential of 0.7 V, which indicate a weakness electrocatalytic activity for hydrazine (Fig. S8). While, increasing the proportion (CNTs:ErGO) from 0.5 to 4, the CNTs-ErGO composite film exhibits a remarkably enhancement sensitivity, and then decrease significantly with the continuously increasing the content of CNTs (Fig. S8 (b-g)). The maximum sensitivity of CNTs-ErGO can be obtained under the optimum weight ratio (CNTs:ErGO) of 2:1. Fig. S8 (h) shows the details information of the measured sensitivity and oxidation potential for CNTs-ErGO composite film under different weight ratio (CNTs:ErGO), and the experimental results exhibit that the CNTs-ErGO composite film initially shows an enhancement performance and reduction oxidation potential, which can be attribute to the presence of CNTs. The introduction of CNTs not only overcomes the π-π interactions between individual graphene nanosheets for stacking, provides a more efficient dispersion of gold nanoparticles, but also greatly improves the electron-transfer rate and yields synergic effect [36]. However, when excessive CNTs are mixed into the CNTs-ErGO film, the proportion of ErGO will reduce and lead to the degradation of catalytic performance. Therefore, the appropriate proportion of CNTs can promote the electrocatalytic effects and lower the oxidation potential of CNTs-ErGO film towards hydrazine oxidation. In the current condition, the maximum sensitivity of the CNTs-ErGO composite film can reach to 0.586 μA/μM for hydrazine detection under the optimization proportion (CNTs:ErGO=2:1), and the subsequent experiments were

### 3.3 Electrocatalytic effect of AuNPs/CNTs-ErGO/GCE toward hydrazine

Fig. 4a exhibits the cyclic voltammetry curves of bare GCE, ErGO/GCE, CNTs-ErGO/GCE, AuNPs/GCE, AuNPs/CNTs/GCE and AuNPs/CNTs-ErGO/GEC in the presence of hydrazine. For the bare GCE, it seems that there was no apparent redox peaks appearance under the applied potential range of -0.3 V to 0.8 V in the presence of hydrazine. When the ErGO was modified on GCE, a weak oxidation peak can be observed for hydrazine catalytic at about 0.70 V. The CNTs-ErGO/GCE produced an obvious oxidation peak at the potential of 0.422 V, and the peak current can reach to 315.4 μA. However, the more obvious oxidation peaks can be observed after AuNPs deposition on the above corresponding electrodes (GCE, ErGO/GCE and CNTs-ErGO/GCE). The measured oxidation peak currents for AuNPs/GCE and AuNPs/CNTs/GCE sensors are 131.4 μA (at 0.22 V) and 216.5 μA (at 0.235 V),

respectively. Especially, for the AuNPs/CNTs-ErGO sensor, the electrocatalytic oxidation peak potential decreased to 0.205 V, and the peak current increased to 519.6 μA, which exhibited a higher catalytic current and a lower oxidation potential than the AuNPs/GCE and AuNPs/CNTs/GCE.

In addition, the catalytic activities of as-prepared sensors were evaluated by subtracting the capacitive current from the CV results. As shown in Fig. S10, the current intensity for AuNPs/CNTs-ErGO/GCE, AuNPs/ErGO/GCE and AuNPs/GCE can reach to 344.0 μA, 185.8 μA and 127.7 μA, separately. The measured results indicate that the AuNPs/CNTs-ErGO possesses a higher catalytic activity for hydrazine electro-oxidation, which can be attributed to the synergistic effect between AuNPs and CNTs-ErGO film and also the good electrocatalytic effect of AuNPs. Furthermore, in order to demonstrate the significance of nanoparticle-form of Au, the control experiment was also conducted on AuNPs and Au disk electrode (Fig. S9).

The catalytic response of AuNPs/CNTs-ErGO/GCE sensor was also evaluated by detecting different concentrations of hydrazine. Fig. 4b shows that the peak of oxidation current increased with the increasing concentration of hydrazine from 0 μM to 300 μM, which reveals that the AuNPs/CNTs-ErGO/GCE sensor exhibits good performance towards hydrazine due to the enhanced electrocatalytic and fast electron transfer properties. In addition, the scan rate dependant experiments were also carried out with hydrazine at various scan rates. The $I_p$ exhibits a linear relationship with $\nu^{1/2}$ and the correlation coefficient reaches to 0.998 (Fig. S11), and the results indicate that the nature of the electrocatalytic process is diffusion controlled for hydrazine detection.

### 3.4 Effects of the quantity of AuNPs on hydrazine detection

It is well know that the number and size of the AuNPs can significantly influence the electrochemical performances of the fabricated sensors. Therefore, in order to optimize the electrodeposition conditions of AuNPs, different amount of AuNPs were deposited on the surface of CNTs-ErGO/GCE by controlling the electrodeposition times (5 s, 20 s, 50 s, 80 s, 120 s and 160 s). Fig. S12 shows the amperometric responses curves of all the AuNPs/CNTs-ErGO/GCE sensors for successive addition of hydrazine in 0.1 M PBS (pH=7.4). Evidently, the sensitivity of the fabricated sensors exhibit enhanced sensitivity with the increase of electrodeposition time from 5

s to 80 s. However, the sensitivity will depress as the electrodeposition time further increase to 120 s and 160 s. For this phenomenon, we speculate that a shorter deposition will lead to very few AuNPs loaded on the CNTs-ErGO surface, and a longer deposition will result in larger even aggregated AuNPs (Fig. 3), which are not conducive to the hydrazine electrochemical catalysis. Moreover, the measured results demonstrate that the AuNPs/CNTs-ErGO/GCE sensor exhibits the highest sensitivity after deposition 80 s, which indicates the optimum deposition time of AuNPs at the current conditions.

### 3.5 Amperometric (i-t) response of the AuNPs/CNTs-ErGO/GCE sensor

The amperometric (i-t) experiments were also conducted on the optimized AuNPs/CNTs-ErGO/GCE sensors to investigate the sensitivity, detection limit, response time and linear concentration range. Fig. 5a illustrates the amperometric current response of sensor by successively dropping hydrazine in the range of 0.3-2419 μM at 0.21 V, and the inset image shows the magnified response curve for a lower concentration variation from 0.3 μM to 18.8 μM. When the hydrazine was dropped into the stirred PBS solution, the oxidation current rose steeply to reach a stable value. The AuNPs/CNTs-ErGO/GCE sensor could accomplish 95% of the steady state current within 3 s, which indicates that the sensor has fast amperometric response behaviour. Fig. 5b shows the plot of oxidation current vs. concentration of hydrazine. The linear equation can be defined as y=0.00191x+0.01473, and the estimated correlation coefficient ($R^2$) is found to be 0.9919, which exhibits a good linear response in the range of 0.3-319 μM. Meanwhile, according to the equation of "sensitivity = slope/ electrode area of the sensor" [37-39], the sensitivity of the optimized AuNPs/CNTs-ErGO/GCE sensor is 9.73 $\mu A \cdot \mu M^{-1} \cdot cm^{-2}$, and the calculated minimum detection limit can down to 0.065 μM. A comparison between the sensing performances of the optimized sensor based on AuNPs/CNTs-ErGO/GCE and literature reports is summarized in Table 1. It is noteworthy that the optimized sensor fabricated in our work exhibits high sensitivity, and relatively low detection limit. Moreover, the overall performance is superior comparing with those reported in the literatures.

### 3.6 Selectivity, reproducibility and stability

In order to evaluate the selectivity of the fabricated AuNPs/CNTs-ErGO/GCE sensor towards hydrazine, many cations and anions present in the form of a salt in boilers and in many of the natural water sources, such as $Cu^{2+}$, $Ca^{2+}$, $K^{+}$, $Pb^{2+}$, $SO_4^{2-}$ and $NO_3^{-}$ etc., and glucose were introduced according to the previous report [40]. In the present, two typical amperometric (i-t) response experiments were carried out and the results are shown in Fig. 6. The current response does not vary significantly after injecting 100 μM interferences into 10 μM hydrazine (Fig. 6a), indicating the interferences will not affect the performance of the sensor. Fig. 6b exhibits the amperometric response in 0.1 M PBS which contains 30 μM interference substances. The inset image shows that the sensor exhibits good linearity in 5-300 μM, and the sensitivity of the sensor is calculated to be 9.57 $\mu A \cdot \mu M^{-1} \cdot cm^{-2}$, which is close to the sensitivity of 9.73 $\mu A \cdot \mu M^{-1} \cdot cm^{-2}$ under no interference environment. The measured results demonstrate that the AuNPs/CNTs-ErGO/GCE sensor possesses good selectivity for hydrazine detection.

The reproducibility of the sensor was evaluated by detecting the current response with five AuNPs/CNTs-ErGO electrodes prepared with the same method. The measured results demonstrated that the sensitivity and linearity of the five electrodes almost remained the same, which exhibits that the fabricated sensor has excellent reproducibility (Fig. S13). Furthermore, the stability was tested by conducting amperometric experiments for every 3 days (Fig. 7), and the sensor was stored at 0-5 ℃. The measured results indicate that the standard deviation of the sensitivities is calculated to be 0.17, which proves that the fabricated sensor has good stability.

### 3.7 Sample recovery test

To further determine the reliability of the fabricated AuNPs/CNTs-ErGO/GCE hydrazine sensor, amperometeric response tests were carried out in known concentrations of hydrazine solution. Six hydrazine samples with the concentration of 5, 10, 50, 100, 200 and 300 μM were prepared by tap water. Then the amperometric experiments were carried out on as-prepared samples. The results are listed in Table 2. Those results demonstrated that the AuNPs/CNTs-ErGO/GCE sensor can be used efficiently for determination of hydrazine in real samples.

## 4. Conclusions

We have successfully fabricated AuNPs/CNTs-ErGO/GCE sensor for electrochemical detection of hydrazine. The cyclic voltammetry and amperometric measurements were conducted to optimize the CNTs to ErGO ratio and the deposition quantity of AuNPs for hydrazine detection. Our results showed an optimum sensor performance at a CNTs to ErGO ratio of 2:1and an electrodeposition time of AuNPs of 80 s. Under optimal conditions, our sensors showed a reproducible sensitivity of 9.73 $\mu A \cdot \mu M^{-1} \cdot cm^{-2}$ with a response time less than 3 s and a low detection limit of 0.065 μM. Such good performances could be attributed to the excellent electrocatalytic effect of Au nanoparticles, and the synergistic effect among AuNPs, CNTs and ErGO. We believe that such performances of high sensitivity, fast response, excellent selectivity and good repeatability are promising for hydrazine detection in practical applications.

## Acknowledgements

This work was supported by the National Natural Science Foundation of China (Grant nos. 51205274, 51205276), Shanxi Scholarship Council of China (Grant no. 2013-035), Scientific Activities of Selected Returned Overseas Professionals in Shanxi Province ([2014]95), Shanxi Province Science Foundation for Youths (Grant no. 2013021017-2), Science and Technology Major Project of the ShanXi Science and Technology Department (20121101004) and Key Disciplines Construction in Colleges and Universities of Shanxi (Grant no. [2012]45).

## References

[1] S. Kumar, G. Bhanjana, N. Dilbaghi, A. Umar, Ceram. Int. 41 (2015) 3101-3108.

[2] A. Umar, M. S. Akhtar, A. Al-Hajry, M. S. Al-Assiri, G. N. Dar, M. Saif Islam, Chem. Eng. J. 262 (2015) 588-596.

[3] S. Ameena, M. S. Akhtarb, H. S. Shin, Sens. Actuators B 173 (2012) 177-183.

[4] S. Ameen, M. S. Akhtar, H. S. Shin, Talanta 100 (2012) 377-383.

[5] A. Umar, M. M. Rahman, S. H. Kim, Y. B. Hahn, Chem. Commun. 2 (2008) 166-168.

[6] M. U. A. Prathap, V. Anuraj, B. Satpati, R. Srivastava, J. Hazard. Mater. 262 (2013) 766-774.

[7] M. M. Reidenberg, P. J. Durant, R. A. Harris, G. D.Boccardo, R. Lahita, K. H. Stenzel, Am. J. Med. 75 (1983) 365-370.

[8] S. D. Zelnick, D. R. Mattie, P. C. Stepaniak, Aviat. Space. Envir. Md. 74 (2003) 1285-1291.

[9] Z. Zhao, Y. Sun, P. Li, S. Sang, W. Zhang, J. Hu, K. Lian, J. Electrochem. Soc. 161 (2014) B157-B162.

[10] M. Mazloum-Ardakani, Z. Taleat, H. Beitollahi, H. Naeimi, *Nanoscale* 3 (2011) 1683-1689.

[11] B. Fang, C. H. Zhang, W. Zhang, G. F. Wang, Electrochim. Acta 55 (2009) 178-182.

[12] A. A. Ensafi, B. Rezaei, Talanta 47 (1998) 645-649.

[13] J. W. Mo, B. Ogorevc, X. Zhang, B. Pihlar, Electroanal. 12 (2000) 48-54.

[14] P. V. K. Rao, G. G. Rao, Talanta 20 (1973) 907-910.

[15] C. M. Morenoa, T. Stadler, A. A. Silva, L. C. A. Barbosa, M. E. L. R. Queiroz, Talanta 89 (2012) 369-376.

[16] J. P. Liu, Y. Y. Li, J. Jiang, X. T. Huang, Dalton Trans. 37 (2010) 8693-8697.

[17] C. Zhang, G. Wang, Y. Ji, M. Liu, Y. Feng, Z. Zhang, B. Fang, Sens. Actuators B 150 (2010) 247-253.

[18] J. Zhang, W. Gao, M. Dou, F. Wang, J. Liu, Z. Li, J. Ji, Analyst 140 (2015) 1686-1692.

[19] D. A. Dikin, S. Stankovich, E. J. Zimney, R. D. Piner, G. H. Dommett, G. Evmenenko, S. T. Nguyen, R. S. Ruoff, Nature 448 (2007) 457-460.

[20] X. Feng, Y. Zhang, J. Zhou, Y. Li, S. Chen, L. Zhang, Y. Ma, L. Wang, X. Yan, Nanoscale 7 (2015) 2427-2432.

[21] X. Feng, N. Chen, Y. Zhang, Z.Yan, X. Liu, Y. Ma, Q. Shen, L. Wang, W. Huang, J. Mater. Chen. A 2 (2014) 9178-9184.

[22] S. Takahashi, N. Abiko, J. Anzai, Materials 6 (2013) 1840-1850.

[23] C. Wang, L. Zhang, Z. Guo, J. Xu, H. Wang, K. Zhai, X. Zhuo, Microchim. Acta 169 (2010) 1-6.

[24] S. Mutyala, J. Mathiyarasu, Sens. Actuators B 210 (2015) 692-699.

[25] Z. Guo, M. Seol, M. Kim, J. Ahn, Y. Choi, J. Liu, X. Huang, Nanoscale 4 (2012) 7525-7531.

[26] Y. Ding, Y. Wang, L. Zhang, H. Zhang, C. M. Li, Y. Lei, Nanoscale 3 (2011) 1149-1157.

[27] M. Yang, B. G. Choi, T. J. Park, N. S. Heo, W. H. Hong, S. Y. Lee, Nanoscale 3 (2011) 2950-2956.

[28] R. Devasenathipathy, V. Mani, S. M. Chen, Talanta 124 (2014) 43-51.

[29] X. Qin, Q. Li, M. Abdullah, Asiri, O. Abdulrahman, Al-Youbi, X. Sun, Gold Bull. 47 (2014) 3-8.

[30] V. Mani, A. T. E. Vilian, S. Chen, Int. J. Electrochem. Sci. **7** (2012) 12774-12785.

[31] W. S. Hummers, R. E. Offeman, J. Am. Chem. Soc. 80 (1958) 1339-1339.

[32] V. Mani, B. Devadas, S. Chen, Biosens. Bioelectron. 41 (2013) 309-315.

[33] X. Peng, X. Liu, Carbon 49 (2011) 3488-3496.

[34] K. Sheng, Y. Sun, C. Li, W. Yuan, G. Shi, Sci. Rep. 2 (2012) 247.

[35] S. Stankovich, D. A. Dikin, G. H. B. Dommett, K. M. Kohlhaas, E. J. Zimney, E. A. Stach, R. D. Piner, S. T. Nguyen, R. S. Ruoff, Nature 442 (2006) 282-286.

[36] Z. Zhang, T. Sun, C.n Chen, F. Xiao, Z. Gong, S. Wang, ACS Appl. Mater. Interfaces 6 (2014) 21035-21040.

[37] W. Sultana, S. Ghosh, B. Eraiah, Electroanal. 24 (2012) 1869-1877.

[38] S. K. Mehta, Khushboo, A. Umar, Talanta 85 (2011) 2411-2416.

[39] K. Mehta, K. Singh, A. Umar, G. R. Chaudhary, S. Singh, Electrochim. Acta 69 (2012) 128-133.

[40] W. Sultana, B. Eraiah, H. N. Vasan, Anal. Methods 4 (2012) 4115-4120.

[41] K. N. Han, C. A. Li, M. P. N. Bui, X. H. Pham, G. H. Seong, Chem. Commun. 47 (2011) 938-940.

[42] H. R. Zare, N. Nasirizadeh, Electrochim. Acta 52 (2007) 4153-4160.

[43] H. Behzad, H. Hassan, B. Somayyeh, Anal. Bioanal. Chem. 398 (2010) 1411-1416.

[44] K. Ramachandran, K. J. Babu, G. G. Kumar, A. Kim, D. J. Yoo, Sci. Adv. Mater. 7 (2015) 329-336.

[45] Y. He, J. Zheng, S. Dong, Analyst 137 (2012) 4841-4848.

[46] M. A. Aziz, A. Kawde, Talanta 115 (2013) 214-221.

[47] C. Batchelor-McAuley, C. E. Banks, A. O. Simm, T. G. J. Jonesb, R. G. Compton, Analyst 131 (2006) 106-110.

[48] M. Shamsipur, Z. Karimi, M. A. Tabrizi, A. Shamsipur, Electroanal. 26 (2014) 1994-2001.

[49] F. Xu, L. Zhao, F. Zhao, L. Deng, L. Hu, B. Zeng, Int. J. Electrochem. Sci. 9 (2014) 2832-2847.

[50] S. Kocak, B. AliSen, Sens. Actuators B 196 (2014) 610-618.

[51] A. R. Fakhari, H. Ahmar, H. Hosseini, S. K. Movahed, Sens. Actuators B 213 (2015) 82-91.

[52] P. C. Pandey, A. K. Pandey, Analyst 137 (2012) 3306-3313.

[53] Madhu, B. Dinesh, RSC Adv. 5 (2015) 54379-54386.

[54] S. Dutta, C. Ray, S. Mallick, S. Sarkar, A. Roy, T. Pal, RSC Adv. 5 (2015) 51690-51700.

[55] Y. Liu, Z. Qiu, Q. Wan, Z. Wang, K. Wu, N. Yang, Electroanalysis, 28 (2016) 126-132.

[56] F. Xu, Y. Liu, S. Xie, L. Wang, Anal. Methods 8 (2016) 316-325.

## Figure captions:

Fig. 1. Schematic illustrations of the fabrication process of AuNPs/CNTs-ErGO/GCE sensors.

Fig. 2. SEM images of GO (a) and CNTs (b), the low (c) and high (d) magnification images of CNTs-GO.

Fig. 3. SEM images of as-prepared AuNPs/CNTs-ErGO (CNTs:ErGO=2:1) with different Au particle deposition times: (a) 5s, (b) 20s, (c) 50s, (d) 80s, (e) 120s and (f) 160s.

Fig. 4. (a) CVs of bare GCE, ErGO/GCE, CNTs-ErGO/GCE, AuNPs/CNTs-ErGO/GCE, AuNPs/GCE and AuNPs/ErGO/GCE in presence of 300 μM hydrazine in 0.1 M PBS at 100 mV/s (vs. Ag/AgCl); (b) CVs in the presence of 0, 50, 100, 200 and 300 μM concentrations of hydrazine in 0.1M PBS (pH=7.4) on AuNPs/CNTs-ErGO/GCE sensor at a scan rate of 100 mV/s (vs. Ag/AgCl).

Fig. 5. (a) The amperometric current response of AuNPs/CNTs-ErGO/GCE for successive addition of hydrazine range from 0.3 μM to 2419 μM in 0.1 M PBS (pH=7.4) at the potential of 0.21 V; Inset image (i): amperometric current response of a very lower hydrazine concentration from 0.3 μM to 18.8 μM; (b) is the linear plot of oxidation current plateau value vs. hydrazine concentration; (i): linear plot for the low concentration of 0.3-18.8 μM.

Fig. 6. (a) Responses of AuNPs/CNTs-ErGO/GCE sensors in the presence of hydrazine and typical interference substances (glucose, $Cu^{2+}$, $Ca^{2+}$, $K^{+}$, $Pb^{2+}$, $SO_4^{2-}$ and $NO_3^{-}$). (b) Response of AuNPs/CNTs-ErGO/GCE sensors at 0.21 V in 0.1 M PBS (pH=7.4) containing 30 μM interference substances; Inset image (i): the linear plot of current vs. hydrazine concentration in interference condition.

Fig. 7. Amperometric current (a) and calculated sensitivity (b) of the sensor for sensitivity evaluation, data obtained every three days.

## Table captions:

Table 1. A response comparison of the AuNPs/CNTs-ErGO/GCE sensor with various hydrazine electrochemical sensors.

| **Sensing materials** | **Sensitivity ($\mu A \cdot \mu M^{-1} \cdot cm^{-2}$)** | **Linear range (μM)** | **LOD[A] (μM)** | **Response time (s)** | **Ref.** |
|---|---|---|---|---|---|
| HMWCNT/GCE | 0.933 | 2.0-122.8 | 0.68 | -- | [42] |
| ZnO/Au | 1.6 | 0.066-425 | 0.066 | <3 | [36] |
| rGO/CuO | 3.87 | 0.1-400 | 0.009 | -- | [44] |
| Co-GE[a]/GCE | 0.56 | 0.25-370 | 0.1 | <3 | [45] |
| ZnOnanorod/SWCNT | 0.1 | 0.5-50 | 0.17 | <5 | [39] |
| PSS[b]-Graphene | -- | 3.0-300 | 1.0 | -- | [23] |

| | | | | | |
|---|---|---|---|---|---|
| ZnO/MWCNTs/GCE | 0.2469 | 0.6-250 | 0.18 | <3 | [11] |
| AuNPs/graphite | -- | 25-1000 | 3.07 | -- | [46] |
| Pd/BDD[c] microdisc array | 4.7 | 10-102 | 1.8 | -- | [47] |
| Pd-AuNPs/GCE | 3.35 | 0.1-500 | 0.07 | <10 | [48] |
| Nano-Au/ZnO-MWCNTs/GCE | $0.0428\mu A\cdot\mu M^{-1}$ | 0.5-1800 | 0.15 | <3 | [17] |
| NanoPd-MWCNTs/GCE | 0.146 | 0.1-10 | 0.016 | <3 | [43] |
| AuPdCu-MWCNT/GCE | $1.26\mu A\cdot\mu M^{-1}$ | 0.1-306 | 0.02 | -- | [49] |
| AuNPs/poly (BCP)[d]/CNT/GCE | 0.568 | 0.5-1000 | 0.1 | -- | [50] |
| AuNPs/PDTYB[e]/MWCNTs/GCE | 0.468 | 2-130 | 0.6 | -- | [51] |
| CPE/NiHCF[f]/AuNP | 0.75 | 0.5-900 | 0.1 | -- | [52] |
| GCE/RGO/ZnO-Au | 5.54 | 0.05-5 | 0.018 | <3 | [53] |
| Au@Pd/rGO-GCE | 11.8 | 2-40 | 0.08 | <10 | [54] |
| AuPd/GR/GCE | 1.415 | 0.02-20 | 0.005 | -- | [55] |
| | 0.708 | 20-166.6 | -- | -- | |
| PEDOT-$Cu_xO$ | 0.414 | 0.5-600 | 0.91 | -- | [56] |
| Graphene nanoflakes/GCE | $0.028\mu A\cdot\mu M^{-1}$ | 0.5-7.5 | 0.3 | <3 | [24] |
| AuNPs/rGO/GCE | -- | 5.0-900 | 0.08 | <3 | [29] |
| GO/CNTs/FePc/GCE | 1.67 | 0.5-83.5 | 0.093 | -- | [30] |
| **AuNPs/CNTs-ErGO/GCE** | **9.73** | **0.3-319** | **0.065** | **<3** | **This work** |

GE[a]: Petalage-like grapheme; PSS[b]: Poly(sodium styrenesulfonate); BDD[c]: Boron-doped diamond; poly (BCP)[d]: poly(bromocresol purple); PDTYB[e]: poly (4,5-dihydro-1,3-thiazol-2-ylsulfanyl-3-methyl-1,2-benzenediol); CPE/NiHCF[f] : Carbon paste electrode/nickel hexacyanoferrate; LOD[A]: Limit of Detection.

Table 2. Determination of hydrazine in real samples.

| Sample | Hydrazine added (μM) | Hydrazine found (μM) | Recovery (%) |
|---|---|---|---|
| 1 | 5 | 5.08±0.06 | 101.6 |
| 2 | 10 | 10.2±0.15 | 102.0 |
| 3 | 50 | 49.1±0.60 | 98.20 |
| 4 | 100 | 102.5±2.50 | 102.5 |
| 5 | 200 | 197.1±4.9 | 98.55 |
| 6 | 300 | 306.5±6.8 | 102.1 |



## Highlights

- The AuNPs/CNTs-ErGO hydrazine sensor was prepared combining electrochemical reduction with electrodeposition methods.
- The influence of the quantity of Au nanoparticles and the proportion of CNTs to ErGO were investigated.

- The optimized sensor exhibited high sensitivity, outstanding linear concentration range and low detection limit.
- The as-synthesized sensor shows great application potential for hydrazine detection.

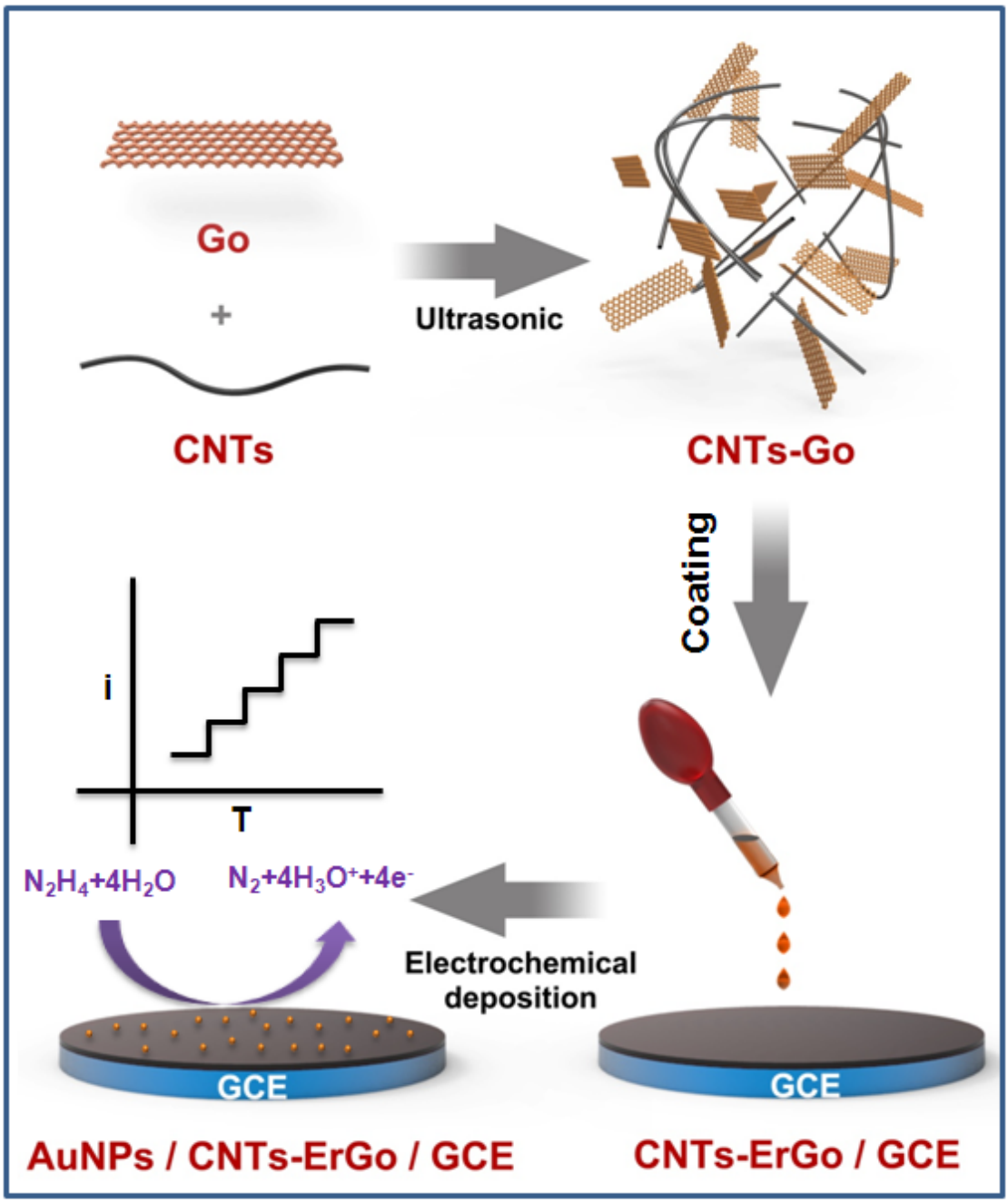
Go
+
CNTs
Ultrasonic
CNTs-Go
Coating
i
T
$N_2H_4+4H_2O$
$N_2+4H_3O^++4e^-$
Electrochemical deposition
GCE
GCE
AuNPs / CNTs-ErGo / GCE
CNTs-ErGo / GCE

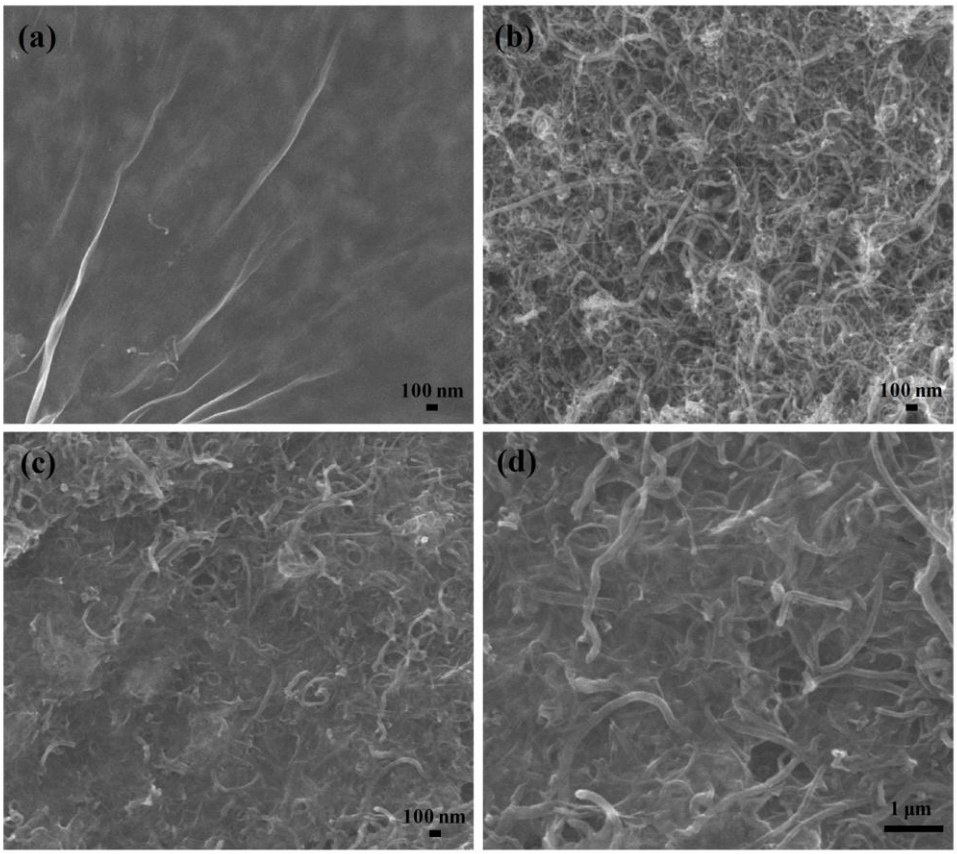

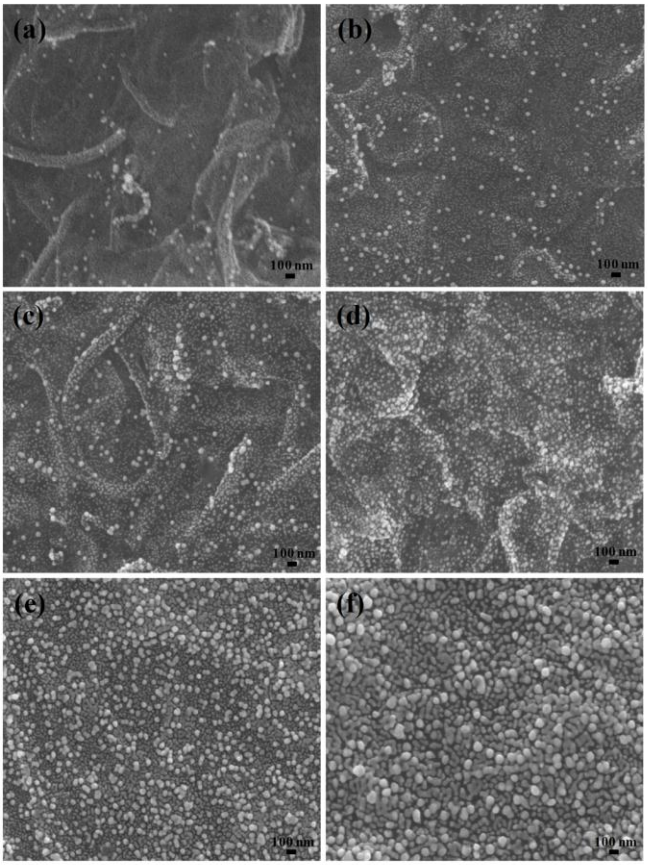
(a)
100 nm
(b)
100 nm
(c)
100 nm
(d)
100 nm
(e)
100 nm
(f)
100 nm

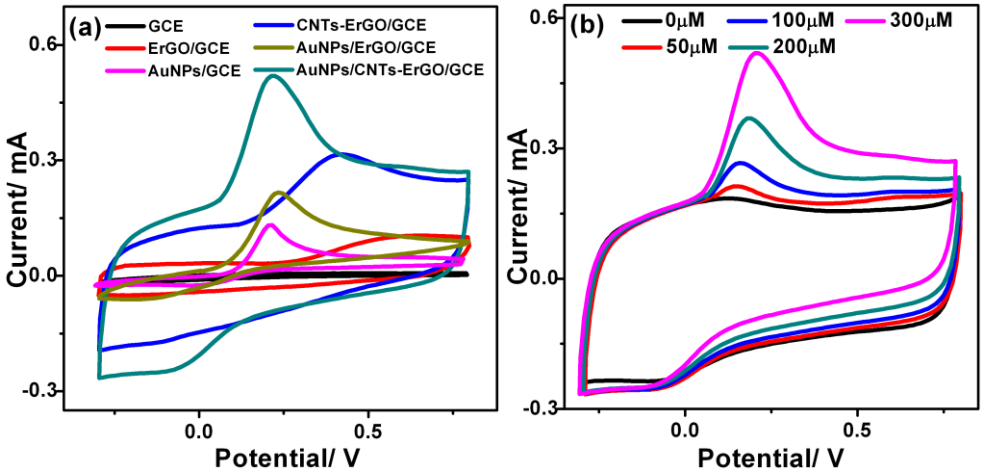
(a)
GCE
ErGO/GCE
AuNPs/GCE
CNTs-ErGO/GCE
AuNPs/ErGO/GCE
AuNPs/CNTs-ErGO/GCE
Current/ mA
Potential/ V
0.6
0.3
0.0
-0.3
0.0
0.5
(b)
0μM
50μM
100μM
200μM
300μM
Current/ mA
Potential/ V